

# Coherent spatial control of wave packet dynamics on quantum lattices

Ilia Tutunnikov,<sup>1</sup> Chern Chuang,<sup>2</sup> and Jianshu Cao<sup>1,\*</sup>

<sup>1</sup>*Department of Chemistry, Massachusetts Institute of Technology, 77 Massachusetts Avenue, Cambridge, Massachusetts 02139, USA*

<sup>2</sup>*Department of Chemistry and Biochemistry, University of Nevada, 4505 S Maryland Pkwy, Las Vegas, Nevada 89154, USA*

Quantum lattices are pivotal in the burgeoning fields of quantum materials and information science. Rapid developments in microscopy and quantum engineering allow for preparing and monitoring wave-packet dynamics on quantum lattices with increasing spatial and temporal resolution. Motivated by these emerging research interests, we present an analytical study of wave packet diffusivity and diffusion length on tight-binding quantum lattices subject to stochastic noise. Our analysis points to the crucial role of spatial coherence and predicts a set of novel phenomena: noise can enhance the transient diffusivity and diffusion length of sufficiently extended initial states; A smooth Gaussian initial state spreads slower than a localized initial state; A standing or traveling initial state with large momentum spreads faster than a localized initial state and exhibits a noise-induced peak in the transient diffusivity; The change in the time-dependent diffusivity and diffusion length relative to a localized initial state follows a universal dependence on the Gaussian width. These theoretical predictions and the underlying mechanism of spatial coherence suggest the possibility of controlling the wave packet dynamics on quantum lattices by spatial manipulations, which will have implications for materials science and quantum technologies.

The rapid advancement in quantum materials and quantum information science has generated renewed interest in quantum lattices [1] of two archetypes: molecular crystals and quantum engineering platforms. Molecular crystals [2] encompass a broad range of organic and inorganic compounds and have demonstrated remarkable potential in charge [3–5] and excited state energy transport [6–16] in terms of tunability and cost-effectiveness. These materials, often characterized by their well-ordered structures, are an ideal platform for quantum coherent control studies. On the other hand, quantum platforms, including optical lattices [17, 18] and superconducting circuits [19–21], offer an entirely different approach to engineering systems for quantum information applications. In particular, such systems can emulate various types of quantum random walks [22–24]. Exploring these two lattice classes extends our understanding of fundamental quantum phenomena and opens new avenues for advancing quantum technologies.

This work delves into the transient diffusivity and diffusion length of spatially extended states on quantum lattices. The confluence of cutting-edge quantum technology and advanced microscopy techniques allows the preparation and observation of quantum phenomena at unprecedented spatial and temporal resolutions [25–28]. Thus, we shift the focus from traditional coherent temporal control [29–35] to spatial coherent control. It is a step toward studying quantum phenomena in solid rather than gaseous phases, including quantum materials.

In this paper, we first introduce various extended wave packets in a tight-binding lattice and then present analytical expressions for their diffusivity and diffusion length in closed and open systems. Our analysis reveals an array of intriguing quantum phenomena, including the noise-induced speed-up and a universal scaling of transient diffusivity and diffusion length with the wave packet width. These findings underscore the crucial role of spatial coherence in the quantum evolution.

**System Definitions and General Formulas.** We examine the dynamics of wave packets on a one dimensional (1D) homogeneous tight-binding lattice, which is an infinite chain of sites with inter-site coupling strength  $J_{m,n}$  between sites  $m$  and  $n$ . The Hamiltonian describing the couplings is

$$\hat{H} = \sum_{m \neq n} J_{m,n} |m\rangle \langle n|, \quad (1)$$

where  $|m\rangle$  and  $|n\rangle$  denote the localized states at sites  $m$  and  $n$ . The physical position of the  $n$ -th site (assuming an equally-spaced lattice) is given by  $x_n = an$ , where  $a$  is the lattice constant. All lengths in this study are normalized to  $a$ . We set  $\hbar = 1$ , and measure time in units of inverse energy.

The primary observable in this study is the time-dependent diffusivity,  $D(t)$  defined as

$$2D(t) = \frac{d\langle n^2(t) \rangle}{dt} - \frac{d\langle n(t) \rangle^2}{dt}, \quad (2)$$

where  $\langle n^k(t) \rangle = \sum_n n^k \rho_{n,n}(t)$ , and  $\rho_{n,n}(t)$  are the diagonal elements of the density matrix. For analytical tractability, we restrict our analysis to nearest-neighbor coupling,  $J_{m,n} = J\delta_{m,n\pm 1}$ . Under this assumption,  $\rho_{n,n}(t)$  satisfy the equation  $\dot{\rho}_{n,n}(t) = 2J\text{Im}[\rho_{n-1,n}(t) + \rho_{n+1,n}(t)]$ , where we used  $\dot{\rho} = -i[H, \rho] = -i(H\rho - \rho H)$ , and  $H$  is the matrix representation of  $\hat{H}$  in the basis of localized states. Spatial coherences and their first moments are defined as ( $l \geq 0$ )

$$\langle \rho(t) \rangle_l = \sum_n \rho_{n,n+l}(t), \quad \langle n(t) \rangle_l = \sum_n n \rho_{n,n+l}(t). \quad (3)$$

In this notation,

$$\frac{d\langle n(t) \rangle}{dt} = \sum_n n \dot{\rho}_{n,n}(t) = 2J\text{Im}[\langle \rho(t) \rangle_1], \quad (4)$$

$$\frac{d\langle n^2(t) \rangle}{dt} = \sum_n n^2 \dot{\rho}_{n,n}(t) = 4J\text{Im}[\langle n(t) \rangle_1] + \frac{d\langle n(t) \rangle}{dt}, \quad (5)$$

where  $J\text{Im}[\langle \rho(t) \rangle_1]$  can be interpreted as population flux, and  $J\text{Im}[\langle n(t) \rangle_1]$  is the displacement-weighted flux.

arXiv:2311.07254v1 [quant-ph] 13 Nov 2023

\* jianshu@mit.edu

When the wave packet center of mass is stationary ( $d\langle n(t)\rangle/dt = 0$ ), the diffusivity simplifies to

$$D(t) = \frac{1}{2} \frac{d\langle n^2(t)\rangle}{dt} = 2J\text{Im}[\langle n(t)\rangle_1], \quad (6)$$

which holds for nearest neighbor coupling even in the presence of noise (considered below).  $\text{Im}[\langle n(t)\rangle_1]$  satisfies the following equation

$$\frac{d\text{Im}[\langle n(t)\rangle_1]}{dt} = \mathcal{S}[\langle n(t)\rangle_1] - J\text{Re}[\langle \rho(t)\rangle_2], \quad (7)$$

where  $\text{Re}[\langle \rho(t)\rangle_2]$  is a measure of spatial coherence. The function  $\mathcal{S}[\langle n(t)\rangle_1]$  varies depending on whether the system is isolated or subject to noise; its explicit forms will be specified later.

We analyze the dynamics of two types of initial states. The first type is a standing Gaussian wave packet with a stationary center of mass, described by

$$\psi_n(0) = \frac{\sqrt{2} \cos(kn)}{\sqrt{w\sqrt{\pi}[1 + e^{-k^2 w^2}]}} \exp\left[-\frac{n^2}{2w^2}\right], \quad (8)$$

where  $k$  is the wave number, and  $w > 0$  is the initial width. The standard Gaussian is obtained by setting  $k = 0$ . The second initial state is the traveling Gaussian

$$\psi_n(0) = \frac{1}{\sqrt{w\sqrt{\pi}}} \exp\left[-\frac{n^2}{2w^2} + ipn\right], \quad (9)$$

where  $p$  is the initial momentum of the wave packet. The traveling Gaussian state describes wave-like propagation and can be relevant for cavity polaritons [36–39]. Here, we restrict the magnitude of  $k$  and  $p$ ,  $0 \leq |k|, |p| \leq \pi/2$ . Extending the values beyond this range yields periodic repetitions of the results.

**Isolated System.** This section focuses on analyzing diffusivity in an isolated system, while the effects of noise will be explored in subsequent sections. In an isolated system,  $\mathcal{S}[\langle n(t)\rangle_1] = J$ , and the spatial coherences are conserved,  $\langle \rho(t)\rangle_l = \langle \rho(0)\rangle_l$ ,  $l \geq 0$ . Consequently, for wave packets with a stationary center of mass, the diffusivity is given by

$$D(t) = D_\delta(t) - 2J^2 \text{Re}[\langle \rho(0)\rangle_2]t, \quad (10)$$

where  $D_\delta(t) = 2J^2 t$  is the well-known diffusivity of Kronecker delta initial state. As indicated by Eq. (10), a positive value of spatial coherence  $\text{Re}[\langle \rho(0)\rangle_2] > 0$  leads to suppressed diffusivity relative to  $D_\delta$ , and vice versa for  $\text{Re}[\langle \rho(0)\rangle_2] < 0$ . For wave packets with a non-stationary center of mass, the expressions for diffusivity and the center of mass are as follows

$$D(t) = D_\delta(t) - 2J^2 (\text{Re}[\langle \rho(0)\rangle_2] + 2\text{Im}[\langle \rho(0)\rangle_1]^2)t + J(\text{Im}[\langle \rho(0)\rangle_1] + 2\text{Im}[\langle n(0)\rangle_1]), \quad (11)$$

$$\langle n(t)\rangle = 2J\text{Im}[\langle \rho(0)\rangle_1]t. \quad (12)$$

Here, without loss of generality, we assume  $\langle n(0)\rangle = 0$ . For detailed derivation and explicit expressions for  $\langle \rho(0)\rangle_{1,2}$  and  $\langle n(0)\rangle_1$  for the considered wave packets, see SI. Note that throughout this work, the sums  $\langle \rho(0)\rangle_{1,2}$  and  $\langle n(0)\rangle_1$

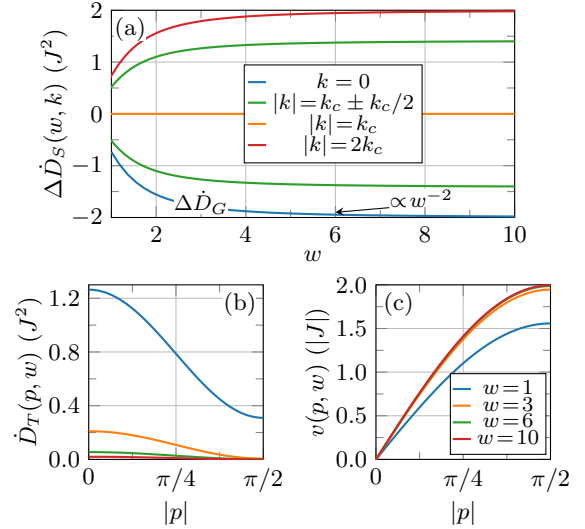


FIG. 1. Isolated system. (a) Derivative of relative diffusivity of a standing Gaussian initial state, see Eq. (16). (b) Derivative of diffusivity of a traveling Gaussian initial state, see Eq. (17). (c) Center of mass velocity, see Eq. (18).

were approximated by integrals. This approximation has a negligible effect for initial states with a width equal to or greater than a single lattice constant  $a$ .

**Isolated system I – Gaussian initial state.**–For the Gaussian initial state,  $\langle \rho(0)\rangle_2 = \exp(-1/w^2)$ , such that

$$D_G(t) = 2J^2(1 - e^{-1/w^2})t, \quad D_G(t) \approx \frac{2J^2}{w^2}t, \quad w \gg 1. \quad (13)$$

The larger the initial width  $w$ , the higher the spatial coherence and the lower the diffusivity. Note that the relative diffusivity is strictly negative  $\Delta \dot{D}_G \equiv \dot{D}_G - \dot{D}_\delta = -2J^2 \exp(-1/w^2) < 0$ , and for  $w \gg 1$ ,  $\Delta \dot{D}_G$  scales as  $w^{-2}$ , as illustrated in Fig. 1(a).

Qualitatively, the decay of diffusivity with increasing  $w$  can be understood in terms of the uncertainty principle. The squared expansion coefficient of the Gaussian state in terms of Bloch states,  $\propto \exp(in\nu)$  is  $|c_\nu|^2 \propto \exp(-w^2\nu^2)$ ,  $\nu \in [-\pi, \pi]$ .  $|c_\nu|^2$  shrinks towards  $\nu = 0$  with increasing  $w$ , while the dispersion relation reads  $E_\nu = 2J \cos(\nu) \approx 2J(1 - \nu^2/2)$ . Consequently, an increase in  $w$  results in reduced energy dispersion among the wave packet’s components, leading to slower spatial spreading. Formally, in the limit  $w \rightarrow \infty$ , the wave packet becomes a soliton—a wave packet that retains its shape. However, this picture is complicated in open systems by the presence of noise, a topic that will be explored in subsequent sections.

Quantitatively, the diffusivity is given by the Green-Kubo formula

$$D_G(t) = \int_0^t \langle v_g(t')v_g(0)\rangle dt' = t \int_{-\pi}^{\pi} v_g^2 |c_\nu|^2 d\nu, \quad (14)$$

where  $v_g(t') \equiv v_g = d_\nu E_\nu = -2J \sin(\nu)$  is the time-independent group velocity of state  $\nu$ , and  $\langle \cdot \rangle$  denotes the weighted average over Bloch states. A sharper distribution  $|c_\nu|^2$  results in a smaller  $\dot{D}_G$ . The integral in Eq. (14) can be explicitly evaluated, thereby reproducing Eq. (13) (see SI for details).

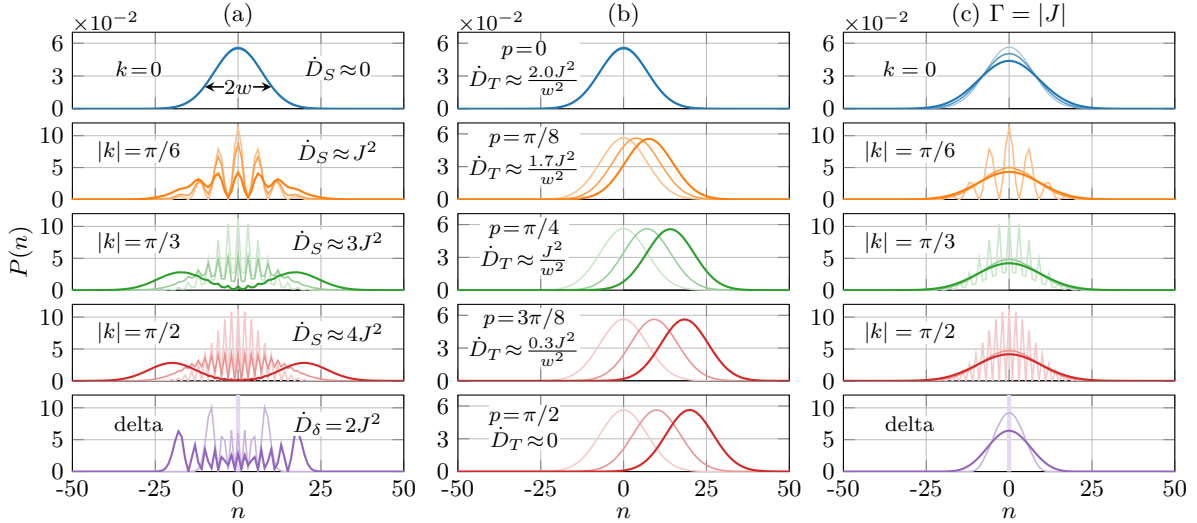


FIG. 2. Population distributions. (a) Isolated system, standing Gaussian. (b) Isolated system, traveling Gaussian. Here  $J < 0$ . (c) Open system (with noise), standing Gaussian. Thin, intermediate, and thick lines correspond to  $t = 0, 5/|J|, 10/|J|$ .  $w = 10$ .

**Isolated system II – Standing Gaussian initial state.**—We now focus on the general case described by Eq. (8), where  $k \neq 0$ . Substituting  $\langle \rho(0) \rangle_2$  for the standing Gaussian initial state into Eq. (10) yields

$$D_S(t) = D_\delta - 2J^2 e^{-1/w^2} \frac{e^{k^2 w^2} \cos(2k) + 1}{e^{k^2 w^2} + 1} t \approx 2J^2 \left[ 1 - e^{-1/w^2} \cos(2k) \right] t; \quad w \gg 1, \quad (15)$$

where  $\langle \rho(0) \rangle_2 \approx \exp(-1/w^2) \cos(2k)$ . Figure 1(a) shows the derivative of relative diffusivity

$$\Delta \dot{D}_S \equiv \dot{D}_S - \dot{D}_\delta \approx -2J^2 e^{-1/w^2} \cos(2k). \quad (16)$$

The expression implies the critical wave number  $|k| = k_c \equiv \pi/4$ , at which  $\Delta D_S$  vanish. For  $|k| > k_c$ ,  $D_S(t)$  is enhanced relative to  $D_\delta(t)$ , and vice versa for  $|k| < k_c$ .

Figure 2(a) depicts the population distributions for a standing Gaussian initial state with  $w = 10$ , evaluated at different times  $t = 0, 5/|J|, 10/|J|$ , and for various values of  $|k|$ . The numerical results confirms the prediction of Eqs. (15) and (16). For the Gaussian state ( $k = 0$ ), there is no visible change on the considered time scale. For  $|k| > 0$ , the wave function  $\psi_n(0) \propto [\exp(ikn) + \exp(-ikn)] \exp[-n^2/(2w^2)]$  gives rise to two wave packets that move in opposite directions with momenta  $\pm k$ . Initially, the overlapping of the two wave packets results in an interference pattern; however, as they separate, this interference diminishes. Similar to the case of a single Gaussian, an increase in the initial width  $w$  leads to reduced energy dispersion and a slower rate of expansion relative to each Gaussian's center of mass. Consequently, when  $w \gg 1$ , the dominant contribution to the diffusivity comes from the relative separation of the two wave packets.

**Isolated system III – Traveling Gaussian initial state.**—We now turn to the traveling Gaussian initial state, as described by Eq. (9), which is similar to one of the two Gaussians in the standing Gaussian state. Substituting  $\langle \rho(0) \rangle_{1,2}$  and  $\langle n(0) \rangle_1$  into Eqs. (11) and (12), yields the

diffusivity  $D_T(t)$  and the center of mass position  $\langle n(t) \rangle$ ,

$$D_T(t) = 2J^2 [1 - e^{-1/w^2} \cos(2p) - 2e^{-1/(2w^2)} \sin^2(p)] t, \quad (17)$$

$$\langle n(t) \rangle = -2J e^{-1/(4w^2)} \sin(p) t. \quad (18)$$

Here, the range of initial momentum magnitude is  $0 \leq |p| \leq \pi/2$ . Figure 1(b) illustrates that an increase in either  $|p|$  or  $w$  leads to suppression of  $\dot{D}_T$ . When  $w \gg 1$ ,

$$\dot{D}_T \approx \frac{J^2}{w^2} [1 + \cos(2p)] \leq \dot{D}_G, \quad (19)$$

which is consistent with the large  $w$  limit of Eq. (13), when  $|p| \ll 1$ . The motion becomes soliton-like for  $|p| = \pi/2$ , i.e., the wave packet retains its shape (refer to SI for a qualitative discussion). Figure 1(c) shows that the speed  $v \equiv |d_t \langle n \rangle|$  is constant over time and increases with both the initial width,  $w$  and  $|p|$ . Figure 2(b) shows population distributions for the traveling Gaussian with  $w = 10$  and several values of  $p$ . There is no visible spreading of the moving wave packet, as the diffusivity is suppressed by the factor of  $w^{-2}$ .

The diffusivities of standing and traveling Gaussian initial states are related by  $D_S(t) = D_T(t) + d_t \langle n(t) \rangle^2 / 2$ , where  $D_S(t)$  is the diffusivity of the standing Gaussian with  $k$  substituted by  $p$  [see Eq. (15)]. This relationship is consistent with the observations illustrated in Fig. 2. In particular, the enhanced diffusivity in the standing Gaussian state is mainly attributed to the relative motion between the two Gaussians, as indicated by the second term, rather than the slower dispersion around each Gaussian's center of mass, which is represented by the first term scaling as  $w^{-2}$ .

**Dynamics in the Presence of Noise: HSR Model.** In this section, we explore the impact of noise on diffusivity within the framework of the Haken-Strobl-Reineker (HSR) model, a well-established approach for the high-temperature regime [40–42]. The model describes site energy fluctuations as white noise. At sufficiently high tem-

peratures, thermal fluctuations dominate over static disorder, allowing us to consider a homogeneous chain. The role of static disorder will be explored in future work [43], particularly in the context of Anderson localization.

Within the HSR model, the density matrix evolves according to the Liouvillian equation [41]

$$\dot{\rho} = -i[H, \rho] - \frac{\Gamma}{2} \sum_{n=-\infty}^{\infty} [V_n, [V_n, \rho]], \quad (20)$$

where the matrix elements of  $V_n$  are  $(V_n)_{j,k} = \delta_{j,n}\delta_{k,n}$ , and  $\Gamma$  is the dephasing rate. Another way of writing Eq. (20) is  $\dot{\rho} = -i[H, \rho] - \Gamma\rho_H$  with  $(\rho_H)_{m,n} = (1 - \delta_{m,n})\rho_{m,n}$ . This form emphasizes the suppression of the off-diagonal elements of the density matrix (coherences), manifesting in exponential decay of spatial coherences,  $\langle \rho(t) \rangle_l = \langle \rho(0) \rangle_l \exp(-\Gamma t)$ ,  $l \geq 1$  (the proof is outlined in SI). In the HSR model,  $\mathcal{S}(\langle n(t) \rangle_1) = J - \Gamma \text{Im}[\langle n(t) \rangle_1]$  [see Eq. (7)], such that

$$\frac{d\text{Im}[\langle n(t) \rangle_1]}{dt} = J - \Gamma \text{Im}[\langle n(t) \rangle_1] - J \text{Re}[\langle \rho(t) \rangle_2]. \quad (21)$$

This is a closed-form equation, amenable to analytical solutions. For real initial states with stationary center of mass, we obtain the generalized form of Eq. (10)

$$\begin{aligned} D_S(t) &= D_\delta(t) - 2J^2 \text{Re}[\langle \rho(t) \rangle_2] t \\ &= D_\delta(t) - 2J^2 \text{Re}[\langle \rho(0) \rangle_2] e^{-\Gamma t} t. \end{aligned} \quad (22)$$

In the presence of noise,  $D_\delta$  is given by [8]

$$D_\delta(t) = 2J^2 \frac{1 - e^{-\Gamma t}}{\Gamma}. \quad (23)$$

On short time scale ( $\Gamma t \ll 1$ ), the effect of dephasing is negligible, and one recovers the ballistic behavior i.e.,  $D_\delta(t) \propto t$ . The coherence is completely lost in the long time limit, leading to a constant diffusivity,  $D_\delta(t \rightarrow \infty) = 2J^2/\Gamma$ .

**Open system I – Gaussian initial state.**–For the Gaussian initial state,  $\langle \rho(0) \rangle_2 = \exp(-1/w^2)$ , and substitution into Eq. (22) yields

$$D_G(t) = 2J^2 \left[ \frac{1 - e^{-\Gamma t}}{\Gamma} - e^{-1/w^2} e^{-\Gamma t} t \right]. \quad (24)$$

- On the short time scale ( $\Gamma t \ll 1$ ), the diffusivity simplifies to that given by Eq. (13).
- In the long-time limit, the diffusivity reaches a steady-state value of  $D_G(t \rightarrow \infty) = 2J^2/\Gamma$ , independent of the initial width  $w$ .
- As in the isolated system  $D_G(t)$  remain smaller than  $D_\delta(t)$ ,

$$\Delta D_G(t) \equiv D_G(t) - D_\delta(t) = -2J^2 e^{-1/w^2} e^{-\Gamma t} t \leq 0. \quad (25)$$

This difference also depends on  $w$  through factor  $\exp(-1/w^2)$ .

Figure 3 shows  $D_G(t)$  for several dephasing rates  $\Gamma$ . For narrow initial states, such as  $w = 1$ , noise acts to suppress

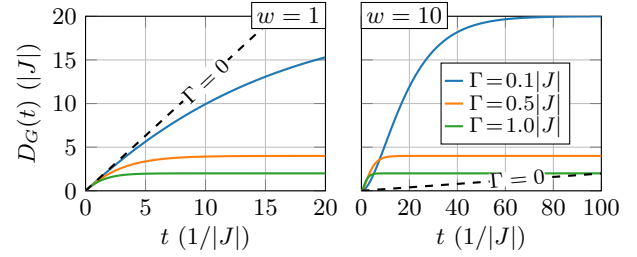


FIG. 3. Diffusivity in the presence of noise for Gaussian initial state of width  $w$ , see Eq. (24).

diffusivity. Conversely, for wider states like  $w = 10$ , diffusivity experiences a transient enhancement. This behavior is in striking contrast to the diffusivity suppression with increasing  $w$  in the isolated system. The *noise-induced enhancement of transient diffusivity* in relatively wide initial states is one of the main results of this letter.

The critical width  $w_c$  for observing an enhancement in diffusivity can be determined by examining the sign of  $\Delta_\Gamma D_G \equiv D_G(t, \Gamma \neq 0) - D_G(t, \Gamma = 0)$ . For  $\Gamma t \ll 1$ , the expression simplifies to  $\Delta_\Gamma D_G \approx \Gamma J^2 t^2 [2 \exp(-1/w^2) - 1]$ , such that

$$w_c = \frac{1}{\sqrt{\ln(2)}} \approx 1.2. \quad (26)$$

**Open system II – Standing Gaussian initial state.**–For the standing Gaussian initial state,  $\langle \rho(t) \rangle_2 = \langle \rho(0) \rangle_2 \exp(-\Gamma t) \approx \exp(-1/w^2) \cos(2k) \exp(-\Gamma t)$ , such that

$$\begin{aligned} D_S(t) &= D_\delta - 2J^2 e^{-1/w^2} \frac{e^{k^2 w^2} \cos(2k) + 1}{e^{k^2 w^2} + 1} e^{-\Gamma t} t \\ &\approx 2J^2 \left[ \frac{1 - e^{-\Gamma t}}{\Gamma} - e^{-1/w^2} \cos(2k) e^{-\Gamma t} t \right], \quad w \gg 1. \end{aligned} \quad (27)$$

The critical width  $w_c$  now depends on the wave number  $k$

$$w_c \approx \frac{1}{\sqrt{\ln[2 \cos(2k)]}}. \quad (28)$$

Noise-induced enhancement is achievable only when  $|k| < \pi/6$ .

Fig. 4(a) shows  $D_S(t)$  for a range of  $|k|$  values. On the short time scale ( $\Gamma t \ll 1$ ), the diffusivity is consistent with Eq. (15). On the long time scale, regardless of the initial state,  $D_S \rightarrow 2J^2/\Gamma$ . For  $|k| \leq \pi/6$  ( $|k| = 0, 0.4$ ), there is transient diffusivity enhancement where the solid lines are above the corresponding dotted lines.

For  $|k| > k_c \equiv \pi/4$ ,  $D_S(t)$  exhibits a peak at  $t_p \approx [1 - \exp(1/w^2) \sec(2k)]/\Gamma$ . This peak is most pronounced when  $|k| = 2k_c$ , occurring at  $t_p = [1 + \exp(1/w^2)]/\Gamma$ . Wave number  $2k_c$  corresponds to a wave length of four lattice spacings, manifesting in destructive interference in spatial coherence. The peak signifies the transition from ballistic wave packet expansion to the steady-state diffusion. For  $|k| > k_c$ , the standing Gaussian initially expands more rapidly than the Kronecker delta. Dephasing, however, takes over eventually, lowering the diffusivity towards the steady-state value. The relative diffusivity is given by

$$\Delta D_S(t) \equiv D_S(t) - D_\delta(t) = -2J^2 e^{-1/w^2} \cos(2k) e^{-\Gamma t} t. \quad (29)$$

It depends on  $w$  through the factor  $\exp(-1/w^2)$ , analogous to the Gaussian case described by Eq. (25). Figure 4(b) shows  $\Delta D_S(t)$  corresponding to panel (a). Once again, we see that for  $|k| > k_c$  the diffusivity is enhanced relative to  $D_\delta$ , and vice versa for  $|k| < k_c$ .

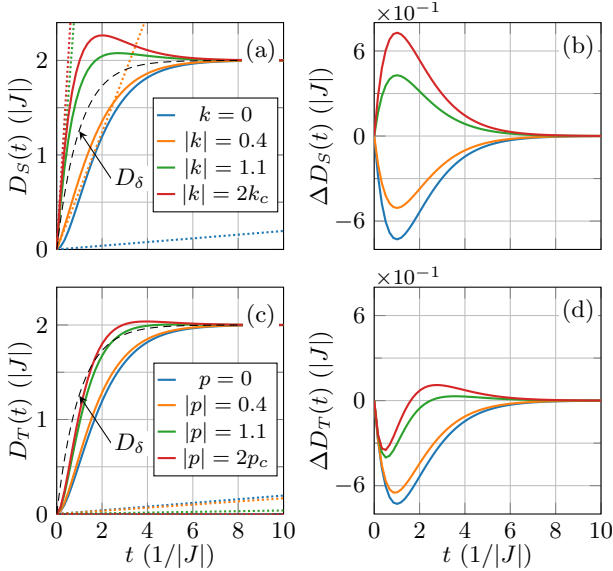


FIG. 4. Diffusivity and relative diffusivity in the presence of noise. (a, b) Standing Gaussian initial state, see Eqs. (27) and (29). (c, d) Traveling Gaussian initial state, see Eq. (30).  $w = 10$ ,  $\Gamma = |J|$ . The corresponding diffusivities in the isolated system ( $\Gamma = 0$ ) are shown by dotted lines in (a) and (c).

The dynamics of population distribution in the presence of noise, as illustrated in Fig. 2(c), also differs from the isolated system. For dephasing rate value of  $\Gamma = |J|$ , noise quickly annihilates spatial coherence and by the time  $t = 5/|J|$ , the distributions for all  $|k|$  values smooth out.

**Open system III – Traveling Gaussian initial state.**—For the traveling Gaussian initial state, the diffusivity and the center of mass position expressions are (for details, see SI)

$$D_T(t) = 2J^2 \frac{1 - e^{-\Gamma t}}{\Gamma} - 2J^2 e^{-1/w^2} \cos(2p) e^{-\Gamma t} - \frac{4J^2}{\Gamma} e^{-1/(2w^2)} \sin^2(p) (1 - e^{-\Gamma t}) e^{-\Gamma t}, \quad (30)$$

$$\langle n(t) \rangle = -\frac{2J}{\Gamma} e^{-1/(4w^2)} \sin(p) (1 - e^{-\Gamma t}). \quad (31)$$

On the short time scale ( $\Gamma t \ll 1$ ), the center of mass moves with a constant velocity, consistent with the isolated system, see Eq. (18). However, the center of mass motion halts due to noise once  $\langle n(t \rightarrow \infty) \rangle = (-2J/\Gamma) \exp[-1/(4w^2)] \sin(p)$  is reached. A larger initial momentum magnitude  $|p|$  and width  $w$  allow the center of mass to travel a greater distance. While in the isolated system the traveling Gaussian shows a soliton-like motion for  $p = \pi/2$ , the center of mass motion slows down in the presence of noise. Moreover, the diffusivity tends to  $p$ -independent steady-state value.

Figure 4(c) shows  $D_T(t)$  for several  $|p|$  values. The critical width for the traveling Gaussian depends on  $|p|$ ,

and varies between  $w_c(p = 0) = [\ln(2)]^{-1/2} \approx 1.2$  [see Eq. (26)] and  $w_c(|p| = \pi/2) = [2 \ln(3 + \sqrt{7})]^{-1/2} \approx 0.54$ . Thus,  $w = 10$  in Fig. 4 is well above the critical width for all  $|p|$  values. The diffusivity does not necessarily approach the steady-state limit in a monotonic fashion. For  $|p| > p_c \equiv \pi/4$ ,  $D_T(t)$  has a peak. The peak is most pronounced for  $p = 2p_c$  with  $t_p \approx 3.92/\Gamma$ . Figure 4(d) show  $\Delta D_T(t)$  corresponding to panel (c). Relative to diffusivity of a delta function initial state, the diffusivity may be transiently enhanced for  $|p| > p_c$  or suppressed for  $|p| < p_c$ .

**Diffusion Length.** Another experimental observable that measures the expansion of finite width initial states is the diffusion length,  $L$  [44, 45]. To define  $L$ , consider the relative mean square displacement (MSD),  $R^2(t) = \langle n^2(t) \rangle - \langle n^2(0) \rangle$ , which is related to the diffusivity by  $R^2(t) = \int_0^t 2D(t') dt'$ . In realistic scenarios, an exciton has a finite lifetime due to both radiative and non-radiative decay mechanisms. For simplicity, we model the exciton lifetime  $t$  as a Poisson process with an exponential distribution  $P(t) = \tau^{-1} \exp(-t/\tau)$ , where  $\tau \geq 0$  is the average lifetime.  $L^2$  is defined as the average of  $R^2(t)$ ,

$$L^2 = \int_0^\infty R^2(t) P(t) dt. \quad (32)$$

In the presence of noise,  $L^2$  of a Gaussian initial state is given by

$$L^2 = 2 \int_0^\infty \int_0^t [D_\delta(t') - 2J^2 \text{Re}[\langle \rho(t') \rangle_2] t'] P(t) dt' dt, \quad (33)$$

where we used Eq. (22), with  $\langle \rho(t) \rangle_2 = \langle \rho(0) \rangle_2 \exp(-\Gamma t) = \exp(-1/w^2) \exp(-\Gamma t)$ , and  $D_\delta(t)$  from Eq. (23). Explicitly,

$$L^2 = 4J^2 \tau^2 \frac{1 + \Gamma \tau - e^{-1/w^2}}{(\Gamma \tau + 1)^2}. \quad (34)$$

Figure 5(a) shows  $L^2$  as functions of  $\Gamma$  for an average lifetime  $\tau = 5/|J|$  and several initial widths  $w$ . When  $\Gamma/|J| \ll 1$ , the diffusivity is suppressed as  $w$  increases due to growing spatial coherence  $\langle \rho(0) \rangle_2 = \exp(-1/w^2)$ . However, for sufficiently wide initial states [ $w > w_c$ , as per Eq. (26)], noise can transiently enhance diffusivity, as shown in Fig. 3, leading to non-monotonic behavior in  $L^2$ . When  $w > w_c$ ,  $L^2$  has a maximum at  $\Gamma_m = [2 \exp(1/w^2) - 1]/\tau$ . In the limit  $\Gamma \tau \gg 1$ ,  $L^2$  becomes independent of  $w$ , and the diffusive transport,  $L^2 \propto \tau/\Gamma$  is recovered.

To compare the diffusion lengths of a Gaussian and Kronecker delta initial states, we consider the relative diffusion length

$$\Delta L^2 \equiv L^2 - L_\delta^2 = -4J^2 e^{-1/w^2} \frac{\tau^2}{(\Gamma \tau + 1)^2}. \quad (35)$$

$\Delta L^2$  is proportional to the spatial coherence  $\langle \rho(0) \rangle_2 = \exp(-1/w^2)$ , consistent with  $\Delta D_G$  in Eq. (25). Figure 5(b) shows  $\Delta L^2$  as a function of  $\Gamma$  for a fixed average lifetime  $\tau = 5/|J|$  and several initial widths  $w$ . For negligible dephasing rate,  $\Gamma \ll |J|$ , we recover the isolated system limit, where  $\langle \rho(0) \rangle_2$  suppresses diffusivity with increasing

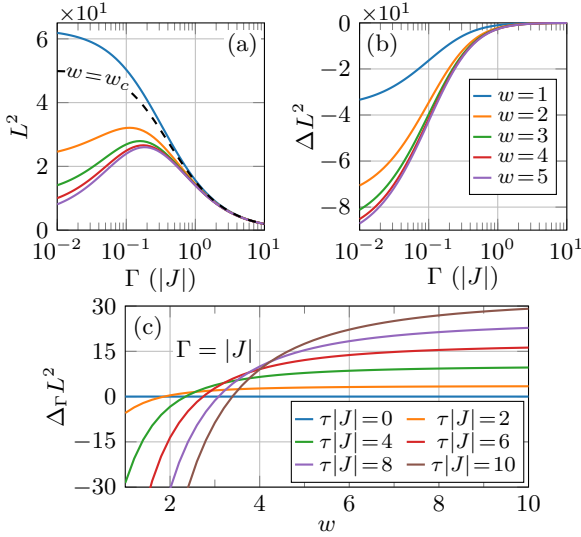


FIG. 5. (a) Squared diffusion length of a Gaussian initial state of width  $w$ , see Eq. (34).  $w_c = [\ln(2)]^{-1/2}$ , see Eq. (26). (b) Relative diffusion length,  $\Delta L^2$  [see Eq. (35)]. In (a) and (b),  $\tau|J| = 5$ . (c) Relative diffusion length,  $\Delta_\Gamma L^2$ .

$w$ . In this regime, the diffusion length of a Gaussian is significantly lower compared to the Kronecker delta. For intermediate values of  $\Gamma$ , noise allows the wave packet to expand more efficiently, approaching the size reached by the Kronecker delta initial state for the same average exciton lifetime. When  $\Gamma \gg |J|$ , the differences between various initial states become negligible.

Next, we examine the gain in diffusion length due to noise using  $\Delta_\Gamma L^2 \equiv L^2(\Gamma) - L^2(0)$ ,

$$\Delta_\Gamma L^2 = 4\Gamma J^2 \tau^3 \frac{(2 + \Gamma\tau)e^{-1/w^2} - (\Gamma t + 1)}{(\Gamma\tau + 1)^2}, \quad (36)$$

Figure 5(c) shows the behavior of  $\Delta_\Gamma L^2$  as a function of  $w$  for various average lifetimes  $\tau$ . For a given  $\tau$ ,  $\Delta_\Gamma L^2$  is positive if  $w$  is sufficiently large, i.e.,

$$e^{-1/w^2} > \frac{1 + \Gamma\tau}{2 + \Gamma\tau}. \quad (37)$$

Note that for  $\Gamma\tau \ll 1$ , we recover the critical width  $w_c$  in Eq. (26). The behavior of  $\Delta_\Gamma L^2$  is consistent with Fig. 3, where the diffusivity in the presence of noise surpasses that in the isolated system for  $w > w_c$ . For example, consider the curve corresponding to  $w = 10$  and  $\Gamma = |J|$  in the right panel. In this specific scenario, the longer the wave packet propagates in the noisy system, the further it will diffuse compared to what would occur in a closed system.

**Conclusions.** In summary, our analytical study of transient diffusivity on quantum lattices provides a wealth of predictions, suggesting new experiments in support of the concept of the spatial coherent control.

1. In comparison with a localized excitation, the finite width of the initial state  $w$  introduces spatial coherence and affects the time-dependent diffusivity. In both closed and open systems, the difference between diffusivity of a

localized state and a finite-width wave packet scales as  $\exp(-a^2/w^2)$ , where  $a$  is the lattice constant.

2. Gaussian or a standing wave packet with long-wavelength modulation [ $0 \leq |k| < \pi/(4a)$ ] expands slower than a delta function (width-suppressed diffusivity), and vice versa for a small-wavelength modulation [ $\pi/(4a) < |k| \leq \pi/(2a)$ ] (width-enhanced diffusivity).
3. Comparing a closed and an open systems, noise can enhance transient diffusivity of a Gaussian wave packet (including a traveling one) of width  $w > w_c$ . The critical width  $w_c$  is found to be of the order of  $a$  ( $w_c \sim a$ ), which is satisfied under realistic optical experimental conditions. In case of a standing wave, the critical width depends on the wave number, and noise enhancement is possible only for  $|k| < \pi/(6a)$ .
4. For a standing or traveling Gaussian wave packet exposed to environmental noise, we establish a critical wave number/momentum value of  $\pi/(4a)$ , beyond which the transient diffusivity exhibits a peak on an intermediate time scale and exceeds the diffusivity of the initially localized wave packet.
5. As the traveling wave packet's initial momentum magnitude  $|p|$  increases, the center of mass motion speeds up, but the dispersion (i.e., the diffusivity) decreases. When the momentum reaches the maximal value  $\pi/(2a)$ , the noise-free wave packet becomes dispersion-less, akin to a soliton.
6. The transient wave packet dynamics can be relevant on the time scale of the exciton lifetime and the length scale of the diffusion length. We explored this connection by computing the unusual dependence of the exciton diffusion length on the initial width, dephasing rate, and exciton lifetime.

These theoretical predictions can be understood from two complementary perspectives: a real space picture and a momentum space picture. (i) The spatial coherence is negatively correlated with the transient diffusion. A smooth wave packet (with long-wavelength modulation) has a positive spatial correlation due to constructive interference and thus suppresses the diffusivity. In contrast, a phase-modulated wave packet (with a short wavelength) has a negative spatial coherence due to destructive interference and can enhance diffusivity. The increase in the wave packet width enhances the magnitude of the spatial coherence and, thus, the change in the transient diffusivity relative to the localized initial state. Furthermore, noise destroys spatial coherence and thus suppresses the effects of spatial modulation. The noise-induced decay of the spatial coherence results in rich and complex behavior in the wave-packet diffusivity. (ii) We can also invoke the momentum representation and uncertainty principle. In general, the spatial profile of a wave packet can be transformed into a momentum distribution. Each momentum component propagates with the group velocity determined by the dispersion relation, and the propagation of the momentum distribution defines the diffusivity and average velocity. This

physical picture is beneficial to understanding the diffusivity of standing and traveling wave packets and the relationship between the two.

Our predictions suggest various possibilities to coherently control the wave packet dynamics on quantum lattices and have implications for materials science and quantum technologies. Time-resolved imaging [25–28] of exciton dynamics on quantum dot superlattices [16, 46] reveals surprising behaviors in both the long-time and transient diffusivities, suggesting the possibility of spatially controlling exciton wave packets. Our analysis of the traveling wave packet can also find its relevance in polariton transport in optical cavities [36–39]. While optical excitation spreads over many lattice spacings, often exceeding the critical width of  $w_c$ , quantum technology platforms such as optical lattices [17, 18] and super-conducting circuits [19–21] can achieve local excitation and fine-tune the initial spreading and spatial modulation, rendering stringent

experimental tests of our predictions. These new experiments motivate the extension of our study to disordered higher-dimensional lattices coupled to phonons [11, 15].

### Associated Content

Supporting information contains derivation details of various diffusivity formulas and auxiliary figures.

### ACKNOWLEDGMENTS

The work is supported by the NSF (Grants No. CHE1800301 and No. CHE2324300), and the MIT Sloan fund. We acknowledge helpful discussions with Eric Heller, Libai Huang, Oliver Kuhn, and Keith Nelson.

- 
- [1] C. M. Goringe, D. R. Bowler, and E. Hernández, Tight-binding modelling of materials, *Rep. Prog. Phys.* **60**, 1447 (1997).
- [2] V. May and O. Kühn, *Charge and Energy Transfer Dynamics in Molecular Systems* (AIP Publishing, 2011).
- [3] N. Karl, K.-H. Kraft, J. Marktanner, M. Münch, F. Schatz, R. Stehle, and H.-M. Uhde, Fast electronic transport in organic molecular solids?, *J. Vac. Sci. Technol. A* **17**, 2318 (1999).
- [4] V. Podzorov, E. Menard, A. Borissov, V. Kiryukhin, J. A. Rogers, and M. E. Gershenson, Intrinsic charge transport on the surface of organic semiconductors, *Phys. Rev. Lett.* **93**, 086602 (2004).
- [5] T. Sakanoue and H. Sirringhaus, Band-like temperature dependence of mobility in a solution-processed organic semiconductor, *Nat. Mater.* **9**, 736 (2010).
- [6] R. Silbey, Electronic energy transfer in molecular crystals, *Annu. Rev. Phys. Chem.* **27**, 203 (1976).
- [7] T. E. Dykstra, E. Hennebicq, D. Beljonne, J. Gierschner, G. Claudio, E. R. Bittner, J. Knoester, and G. D. Scholes, Conformational Disorder and Ultrafast Exciton Relaxation in PPV-family Conjugated Polymers, *J. Phys. Chem. B* **113**, 656 (2009).
- [8] J. M. Moix, M. Khasin, and J. Cao, Coherent quantum transport in disordered systems: I. The influence of dephasing on the transport properties and absorption spectra on one-dimensional systems, *New J. Phys.* **15**, 085010 (2013).
- [9] C. J. Bardeen, The Structure and Dynamics of Molecular Excitons, *Annu. Rev. Phys. Chem.* **65**, 127 (2014).
- [10] C. K. Lee, J. Moix, and J. Cao, Coherent quantum transport in disordered systems: A unified polaron treatment of hopping and band-like transport, *J. Chem. Phys.* **142**, 164103 (2015).
- [11] C. Chuang, C. K. Lee, J. M. Moix, J. Knoester, and J. Cao, Quantum diffusion on molecular tubes: Universal scaling of the 1d to 2d transition, *Phys. Rev. Lett.* **116**, 196803 (2016).
- [12] S. Doria, T. S. Sinclair, N. D. Klein, D. I. G. Bennett, C. Chuang, F. S. Freyria, C. P. Steiner, P. Foggi, K. A. Nelson, J. Cao, A. Aspuru-Guzik, S. Lloyd, J. R. Caram, and M. G. Bawendi, Photochemical control of exciton superradiance in light-harvesting nanotubes, *ACS Nano* **12**, 4556 (2018).
- [13] P. Malý, J. Lüttig, A. Turkin, J. Dostál, C. Lambert, and T. Brixner, From wavelike to sub-diffusive motion: exciton dynamics and interaction in squaraine copolymers of varying length, *Chem. Sci.* **11**, 456 (2020).
- [14] W. Popp, D. Brey, R. Binder, and I. Burghardt, Quantum dynamics of exciton transport and dissociation in multichromophoric systems, *Annu. Rev. Phys. Chem.* **72**, 591 (2021).
- [15] C. Chuang and J. Cao, Universal Scalings in Two-Dimensional Anisotropic Dipolar Excitonic Systems, *Phys. Rev. Lett.* **127**, 047402 (2021).
- [16] D. D. Blach, V. A. Lumsargis, D. E. Clark, C. Chuang, K. Wang, L. Dou, R. D. Schaller, J. Cao, C. W. Li, and L. Huang, Superradiance and Exciton Delocalization in Perovskite Quantum Dot Superlattices, *Nano Lett.* **22**, 7811 (2022).
- [17] M. Ben Dahan, E. Peik, J. Reichel, Y. Castin, and C. Salomon, Bloch oscillations of atoms in an optical potential, *Phys. Rev. Lett.* **76**, 4508 (1996).
- [18] P. M. Preiss, R. Ma, M. E. Tai, A. Lukin, M. Rispoli, P. Zupancic, Y. Lahini, R. Islam, and M. Greiner, Strongly correlated quantum walks in optical lattices, *Science* **347**, 1229 (2015).
- [19] C. S. Wang, J. C. Curtis, B. J. Lester, Y. Zhang, Y. Y. Gao, J. Freeze, V. S. Batista, P. H. Vaccaro, I. L. Chuang, L. Frunzio, L. Jiang, S. M. Girvin, and R. J. Schoelkopf, Efficient Multiphoton Sampling of Molecular Vibronic Spectra on a Superconducting Bosonic Processor, *Phys. Rev. X* **10**, 021060 (2020).
- [20] M. Gong, S. Wang, C. Zha, M.-C. Chen, H.-L. Huang, Y. Wu, Q. Zhu, Y. Zhao, S. Li, S. Guo, H. Qian, Y. Ye, F. Chen, C. Ying, J. Yu, D. Fan, D. Wu, H. Su, H. Deng, H. Rong, K. Zhang, S. Cao, J. Lin, Y. Xu, L. Sun, C. Guo, N. Li, F. Liang, V. M. Bastidas, K. Nemoto, W. J. Munro, Y.-H. Huo, C.-Y. Lu, C.-Z. Peng, X. Zhu, and J.-W. Pan, Quantum walks on a programmable two-dimensional 62-qubit superconducting processor, *Science* **372**, 948 (2021).
- [21] A. H. Karamlou, J. Braumüller, Y. Yanay, A. Di Paolo, P. M. Harrington, B. Kannan, D. Kim, M. Kjaergaard, A. Melville, S. Muschinske, B. M. Niedzielski, A. Vepsäläinen, R. Winik, J. L. Yoder, M. Schwartz, C. Tahan, T. P. Orlando, S. Gustavsson, and W. D. Oliver, Quantum transport and localization in 1d and 2d tight-

- binding lattices, *npj Quantum Inf.* **8**, 35 (2022).
- [22] A. M. Childs, E. Farhi, and S. Gutmann, An Example of the Difference Between Quantum and Classical Random Walks, *Quantum Inf. Process.* **1**, 35 (2002).
- [23] J. Kempe, Quantum random walks: An introductory overview, *Contemp. Phys.* **44**, 307 (2003).
- [24] O. Mülken and A. Blumen, Spacetime structures of continuous-time quantum walks, *Phys. Rev. E* **71**, 036128 (2005).
- [25] G. M. Akselrod, P. B. Deotare, N. J. Thompson, J. Lee, W. A. Tisdale, M. A. Baldo, V. M. Menon, and V. Bulović, Visualization of exciton transport in ordered and disordered molecular solids, *Nat. Commun.* **5**, 3646 (2014).
- [26] T. Zhu, J. M. Snaider, L. Yuan, and L. Huang, Ultrafast Dynamic Microscopy of Carrier and Exciton Transport, *Annu. Rev. Phys. Chem.* **70**, 219 (2019).
- [27] N. S. Ginsberg and W. A. Tisdale, Spatially Resolved Photogenerated Exciton and Charge Transport in Emerging Semiconductors, *Annu. Rev. Phys. Chem.* **71**, 1 (2020).
- [28] M. Delor, H. L. Weaver, Q. Yu, and N. S. Ginsberg, Imaging material functionality through three-dimensional nanoscale tracking of energy flow, *Nat. Mater.* **19**, 56 (2020).
- [29] D. J. Tannor and S. A. Rice, Control of selectivity of chemical reaction via control of wave packet evolution, *J. Chem. Phys.* **83**, 5013 (1985).
- [30] P. Brumer and M. Shapiro, Control of unimolecular reactions using coherent light, *Chem. Phys. Lett.* **126**, 541 (1986).
- [31] J. Cao, C. J. Bardeen, and K. R. Wilson, Molecular “ $\pi$  Pulse” for Total Inversion of Electronic State Population, *Phys. Rev. Lett.* **80**, 1406 (1998).
- [32] S. A. Rice and M. Zhao, *Optical Control of Molecular Dynamics* (Wiley Inter-science: New York, 2000).
- [33] R. Chakrabarti and H. Rabitz, Quantum control landscapes, *Int. Rev. Phys. Chem.* **26**, 671 (2007).
- [34] D. Tannor, *Introduction to Quantum Mechanics: A Time-Dependent Perspective* (University Science Books, Sausalito, 2007).
- [35] M. Shapiro and P. Brumer, *Quantum Control of Molecular Processes* (Wiley: New York, 2011).
- [36] F. J. Garcia-Vidal, C. Ciuti, and T. W. Ebbesen, Manipulating matter by strong coupling to vacuum fields, *Science* **373**, eabd0336 (2021).
- [37] G. Engelhardt and J. Cao, Unusual dynamical properties of disordered polaritons in microcavities, *Phys. Rev. B* **105**, 064205 (2022).
- [38] J. Cao, Generalized resonance energy transfer theory: Applications to vibrational energy flow in optical cavities, *J. Phys. Chem. Lett.* **13**, 10943 (2022).
- [39] G. Engelhardt and J. Cao, Polariton localization and dispersion properties of disordered quantum emitters in multimode microcavities, *Phys. Rev. Lett.* **130**, 213602 (2023).
- [40] A. Madhukar and W. Post, Exact solution for the diffusion of a particle in a medium with site diagonal and off-diagonal dynamic disorder, *Phys. Rev. Lett.* **39**, 1424 (1977).
- [41] V. M. Kenkre and P. Reineker, *Exciton Dynamics in Molecular Crystals and Aggregates*, 1st ed. (Springer Berlin, Heidelberg, 1982).
- [42] A. Amir, Y. Lahini, and H. B. Perets, Classical diffusion of a quantum particle in a noisy environment, *Phys. Rev. E* **79**, 050105 (2009).
- [43] Work in progress., (2023).
- [44] R. R. Lunt, N. C. Giebink, A. A. Belak, J. B. Benziger, and S. R. Forrest, Exciton diffusion lengths of organic semiconductor thin films measured by spectrally resolved photoluminescence quenching, *J. Appl. Phys.* **105**, 053711 (2009).
- [45] J. D. A. Lin, O. V. Mikhnenko, J. Chen, Z. Masri, A. Ruseckas, A. Mikhailovsky, R. P. Raab, J. Liu, P. W. M. Blom, M. A. Loi, C. J. García-Cervera, I. D. W. Samuel, and T.-Q. Nguyen, Systematic study of exciton diffusion length in organic semiconductors by six experimental methods, *Mater. Horiz.* **1**, 280 (2014).
- [46] D. D. Blach, V. A. Lumsargis, C. Chuang, D. E. Clark, S. Deng, O. F. Williams, C. W. Li, J. Cao, and L. Huang, Environment-Assisted Quantum Transport of Excitons in Perovskite Nanocrystal Superlattices, Submitted (2023).